

## **THESIS**

Steven S. Mink, Captain, USAF AFIT/GE/ENG/06-43

# DEPARTMENT OF THE AIR FORCE AIR UNIVERSITY

# AIR FORCE INSTITUTE OF TECHNOLOGY

Wright-Patterson Air Force Base, Ohio

APPROVED FOR PUBLIC RELEASE; DISTRIBUTION UNLIMITED

The views expressed in this t policy or position of the Unit States Government.	thesis are those of the author atted States Air Force, Departme	nd do not reflect the official ent of Defense, or the United

## **THESIS**

Presented to the Faculty

Department of Electrical and Computer Engineering

Graduate School of Engineering and Management

Air Force Institute of Technology

Air University

Air Education and Training Command

In Partial Fulfillment of the Requirements for the

Degree of Master of Science in Electrical Engineering

Steven S. Mink, BSEE
Captain, USAF

March 2006

APPROVED FOR PUBLIC RELEASE; DISTRIBUTION UNLIMITED

Steven S. Mink, BSEE Captain, USAF

Approved:	
/signed LaVern A. Starman (Chairman)	date
/signed/ James A. Fellows (Member)	date
/signed/ Guna S. Seetharaman (Member)	date

#### **Abstract**

This thesis addresses the development of a new micro-scale interrupter mechanism for a safe and arm device used in modern weapon systems. The interrupter mechanism often consists of a physical barrier that prevents an initial source of energy, in an explosive train, from being transferred to subsequent charges. In general, when the physical barrier is removed, the weapon is considered armed, and the charge is allowed to propagate. Several issues facing current safe and arm devices systems are the shrinking industrial base for manufacturing these devices and the desire for modern safe and arm devices to be compatible with next generation weapon systems that are generally decreasing in size and increasing in complexity. The solution proposed here is to design, fabricate, and test a conceptual interrupter mechanism using Microelectromechanical Systems (MEMS) components. These components have inherent benefits over current devices, such as smaller feature sizes and lower part counts, which have the capability to improve performance and reliability. After an extensive review of existing micro-scale safe and arm devices currently being developed, a preliminary design was fabricated in a polysilicon surface micromachining process. The operating principle of this conceptual interrupter mechanism is to have MEMS actuators slide four overlapping plates away from each other to create an aperture, thus providing an unimpeded path for an initiating energy source to propagate. Operation of the fabricated MEMS interrupter mechanism was successfully demonstrated with an approximate aperture area of 1024 µm<sup>2</sup> being created.

# AFIT/GE/ENG/06-43

To Nicholas and Jeffrey

#### Acknowledgments

This thesis would have been impossible without the daily motivation and encouragement provided by my family. Without their support and patience during the countless long days and nights, this endeavor could never have been completed. I would like to express my gratitude to Major LaVern Starman, my faculty advisor, for his encouraging guidance and patience throughout my endless hours in the lab and at the computer. Furthermore, I am indebted to my other committee members, Lt Col James Fellows and Dr. Guna Seetharaman, for the guidance and assistance they provided, which are reflected in the final product. I would also like to thank Capt Ken Bradley and Mr. Ed Wild, from AFRL/MN, who provided essential details about the slapper design and offered encouraging comments about the final fabricated device. Thanks also goes to Capt Paul Kladitis, whose excitement about MEMS first inspired me in choosing this topic for my research. In addition, Gabriel Safford must be recognized for providing the initial research on micro-scale safe and arm devices while working at AFIT during the summer of 2004.

My fellow classmates, especially Frank Parada and Jeff Clark, deserve a hearty thank you for battling alongside me through the trenches that are AFIT. Without their assistance, the rigors of this experience would have been much more difficult to endure. A special thanks goes to my fellow MEMS warrior, Dan Denninghoff. The results of this work would not have been the same without Dan asking the important question, "What is

it again that this device is supposed to do?" His commitment to the truth and willingness to assist in analyzing the theory behind my research contributed significantly to the thoroughness of this thesis.

I am also grateful to the following list of AFIT professionals: Bill Trop and Rick Patton, whose unwavering laboratory support enabled me to produce most of the data presented in this thesis; the AFIT library personnel, whose amazing document retrieval skills enabled me to acquire critical bits of information that are included throughout this document; and Tetsuo Kaieda for providing me with invaluable laboratory equipment training and offering the type of guidance that could only come from a graduating student. In addition, thanks also goes to the following people outside of AFIT: Antonio Crespo, from AFRL/SNDI, for his assistance in fixing one of my design errors with a focused ion beam; and Steve Topper for making himself available to give my "final" thesis a thorough scrubbing so that the work contained within this document is a much more professional product. Finally, a special thanks goes out to all Ammo troops—past, present, and future—whose never-ending effort goes largely unnoticed.

Steven S. Mink

# **Table of Contents**

		Page
Αł	bstract	iv
Αc	cknowledgments	vi
Lis	st of Figures	x
Lis	st of Tables	xix
1.	Introduction	1-1
1.	muoduction	
	1.1 Safe and Arm Device Functional Description	1-1
	1.2 Problem Statement	
	1.3 Proposed Solution	1-6
	1.4 Conclusion	1-7
	Bibliography	1-9
2.	Background	2-1
	2.1 Fuze Fundamentals	2-1
	2.2 Environmental Factors in Fuze Design	
	2.3 Current Research Efforts on MEMS-Based Safe and Arm Devic	
	2.3.1 Naval Surface Warfare Center – Indian Head Division	2-6
	2.3.2 Naval Air Warfare Center – Weapons Division	
	2.3.3 Armament Research, Development and Engineering Cen	
	2.3.4 Air Force Research Laboratory – Munitions Directorate	
	2.4 Introduction of Design Concept for MEMS S&A Device	2-20
	Bibliography	2-21
3.	Explosive Initiation Devices and Concepts	3-1
	3.1 Explosive Initiation Devices	3-1
	3.2 Exploding Foil Initiator	
	3.3 Solid-State Slapper Detonators	
	3.3.1 Design for Silicon-Based Slapper Detonator	3-7
	3.3.2 Microfabricated Slapper Device	
	3.3.3 Solid-State Slapper Detonator System	
	3.4 Solid-State Slapper Interrupter Concept	3-16
	3.5 Introduction of MEMS S&A Interrupter Concept	3-20
	Bibliography	3-22

4.	De	esign Theory and Fabrication	4	- 1
	4.1	PolyMUMPs Fabrication Process	4.	_ 1
	1.1	4.1.1 Sequential Fabrication Procedures		
		4.1.2 Additional Process Constraints		
	4.2	Interruption Method for the MEMS S&A Interrupte		
	4.3	Electrothermal Actuator Theory		
		4.3.1 Thermal Expansion Theory		
		4.3.2 Electrothermal Actuator Performance Consi		
		4.3.3 Electrothermal Actuator Comparisons		
		4.3.4 Electrothermal Actuator Designed for Interr		
	4.4	Bent-Beam Electrothermal Actuator	-	
		4.4.1 Design Parameter Optimization	4-1	19
		4.4.2 Force Measurement Technique		
	4.5	Interrupter Design Theory		
		4.5.1 Analysis of Interrupter Aperture		
		4.5.2 Required Actuator Force Calculations		
		4.5.3 Additional Considerations		
	4.6	Summary	4-4	12
	Bibl	liography		
5.	Ex	xperimental Procedure and Results	5.	- 1
	<i>7</i> 1		5	1
	5.1	PolyMUMPs Fabrication Process Test Structures		
	5.2	Bent-Beam Electrothermal Actuator Experiments		
		5.2.1 Electrothermal Actuator Deflection Experin		
	<i>5</i> 2	5.2.2 Electrothermal Actuator Force Experiment.		
	5.3	Interrupter Mechanism Tests		
	5.4	Summary		
	Bibl	liography		51
6.	Co	onclusions and Recommendations	6.	_ 1
0.		onerusions and recommendations		1
	6.1	Conclusions and Recommendations Based on Expe	rimental Work6	- 1
		6.1.1 Fabrication Process		
		6.1.2 Stand-Alone Actuators		
		6.1.3 Interrupter Mechanism		
	6.2	Recommendations for Future Work		
		liography		
Ap	pend	lix A. Release Procedures for Microelectromechan	ical Systems A-	- 1
Αŗ	pend	lix B. PolyMUMPs Run Data	B	- 1
A -		liv C Enhanced Design Lavores		1
Αľ	pend	lix C. Fabricated Design Layouts	C·	- 1
Vi	<b>+</b> 0		D	1

# **List of Figures**

Figure	Page
Figure 1-1.	Fuzes currently being used in military weapons [4]. Safe and arm devices are a critical component within each of these fuzes
Figure 1-2.	Schematic diagram of a generic explosive train. The spatial relationship between fuze, S&A device, and other charges is shown
Figure 2-1.	Relative size comparison between CCAT warhead, firing device, and MEMS-based S&A device [7], [8]. Warhead outer diameter is 6.75 in. and the entire S&A package is approximately 1 in. <sup>3</sup> 2-7
Figure 2-2.	Design concept of the 45° edge reflector as an optical switch in both the (a) safe and (b) armed position [11]2-9
Figure 2-3.	(a) Schematic of comb drive actuator used to align the edge reflector with the source fiber. (b) SEM image of fabricated comb drive actuator along with both the source and receiver optical fibers [11]
Figure 2-4.	SEM image of the source and receiver fiber alignment with the gold-coated silicon reflector. The thickness of the reflector is approximately $100~\mu m$ [11].
Figure 2-5.	Exploded view of the distributed S&A system in a conceptual warhead application. Diameter of "smart" detonator package is 13 mm [15]
Figure 2-6.	(a) Schematic diagram of slider mechanism. (b) MEMS slider mechanism shown with significant components labeled [14]2-13
Figure 2-7.	Different detonator initiation schemes provides for a potential aiming capability by directing the blast of the warhead [14]2-14
Figure 2-8.	Operational schematic of the ARDEC S&A device in the safe position [19]2-16
Figure 2-9.	Operational schematic of the ARDEC S&A device in the armed position [19]2-17

Figure 2-10.	(a) Depiction of circular SiC membrane formed over a bulk etched SiC substrate. (b) Stress counter plot of a similar structure under an applied shock load [21].	2-19
Figure 3-1.	Major components used in an Exploding Foil Initiator [1]	3-4
Figure 3-2.	Schematic cross-section of Exploding Foil Initiator showing the sequence of steps during functioning [1].	3-5
Figure 3-3.	Illustration of a proposed silicon slapper detonator design [14]. All layers are deposited using microfabrication techniques, except for the Pyrex glass plate, which is epoxy, bonded during post-processing steps.	3-8
Figure 3-4.	Cross-sectional illustration of proposed silicon slapper detonator [14]. Note the flyer and resulting shock wave depict the slapper after firing has occurred.	3-9
Figure 3-5.	An illustration of the preferential etching of silicon by an anisotropic etchant [7]. To protect the areas where etching is not desirable, a layer of silicon dioxide is deposited to prevent the etchant from making contact with the silicon. The bracketed numbers represent specific crystal directions.	3-10
Figure 3-6.	(a) Illustration of conceptual slapper device fabricated in a silicon substrate with deposited metal conductor. (b) Cross-sectional view of cavity showing deposited metal conductor [7]	3-11
Figure 3-7.	(a) Illustration of conceptual slapper device fabricated in a silicon substrate with diffused impurity atoms. (b) Cross-sectional view of cavity showing diffused impurity atoms [7]	3-12
Figure 3-8.	Conceptual slapper device produced by bonding two separately fabricated semiconductor wafers [7]	3-13
Figure 3-9.	Illustration of both the top and side view of the solid-state capacitor fabricated for the slapper detonator system [15]	3-14
Figure 3-10.	Illustration of the top and side view of both the solid-state capacitor and switch fabricated for the slapper detonator system [15]	3-15

Figure 3-11.	Illustration of the top and side view of the complete solid-state slapper detonator system, including a resistor to bleed stray charges in the capacitor, and an external circuit used for driving the trigger switch [15]	. 3-17
Figure 3-12.	Depiction of explosive train interruption by moving the HE pellet out-of-line with the initiating flyer material [15]. The in-line (armed) position in shown.	.3-18
Figure 3-13.	Conceptual illustration of an explosive train interruption method using a slidable barrel. (a) Depicts the barrel in the safe position. (b) Depicts the barrel in the armed position [2]	. 3-19
Figure 3-14.	Conceptual design for the integration of a MEMS interrupter mechanism with a solid-state slapper detonator. This is a modification of the concept proposed by Henderson et al. [7] and shown in Figure 3-8.	3-21
Figure 4-1.	Cross-sectional illustration of the PolyMUMPs process (not to scale) [1]. The numbers below the layers represent nominal layer thicknesses and the blue text represents oxide layer etches performed during processing.	4-3
Figure 4-2.	Illustration of the released PolyMUMPs structure [1] depicted in Figure 4-1. Note that the sacrificial oxide layers have been etched away by the 48% HF solution.	4-5
Figure 4-3.	Design layout used to determine the minimum fabrication width, $w$ , of all three polysilicon layers. The numbers to the right represent the designed width of each structure, in $\mu$ m, with the last structure being 0.5 $\mu$ m and the second to last structure being 1.0 $\mu$ m. Note: the black dots represent a 10 $\mu$ m reference grid used in the design layout tool, and the dark vertical bars on the Poly1 and Poly 2 are Anchor1 and Anchor2 etches, respectively.	4-6
Figure 4-4.	Design layout used to determine minimum spacing, s, between similar material layers. The numbers to the right represent the spacing between the two adjacent structures, in µm. Again, the black dots represent a 10 µm reference grid, and the dark vertical bars are Anchor1 (Poly1) and Anchor2 (Poly2) etches.	4-7
Figure 4-5.	Optical profiler used to obtain vertical measurements of fabricated MEMS structures	4-8

Figure 4-6.	Design layout of the entire MEMS S&A interrupter device. The green arrows in the center represent the direction of motion upon actuation. The entire device covers an area less than 2.1 mm <sup>2</sup>	4-9
Figure 4-7.	SEM image of the fabricated MEMS S&A interrupter device from the design layout shown in Figure 4-6. Again, the green arrows represent the direction of actuator motion when power is applied. Also, note that the entire device is smaller than the 3.8 mm <sup>2</sup> die	4-10
Figure 4-8.	Simple schematics of two electrothermal actuators considered for use with the interrupter mechanism fabricated in this research effort. (a) U-shaped actuator showing in-plane arcing motion. (b) Bent-beam actuator showing linear in-plane motion.	4-11
Figure 4-9.	Thermal expansion of a beam due to Joule heating. The coefficient of thermal expansion associated with the specific beam material will be a key factor in determining the change in length. The other contributing factor is the current per cross-sectional area, A, that will produce a temperature change throughout the beam [6], [7]	4-12
Figure 4-10.	Measured deflection versus power input for an electrothermal ushaped actuator fabricated in the PolyMUMPs process. Data points come from five identical actuators [13].	4-16
Figure 4-11.	A simplified bent-beam actuator showing the basic design parameters of pre-bend angle, $\theta$ , and arm length, $L$ . Note: that $\theta$ is exaggerated for illustrative purposes.	4-17
Figure 4-12.	Results of deflection versus pre-bend angle tests performed on 2- µm thick polysilicon bent-beam electrothermal actuators [8]. The maximum deflection was observed for a pre-bend angle of 1.05°	4-21
Figure 4-13.	Modeled temperature distribution profile showing two bent-beam actuators – straight arms (P1-SU) and tapered arms (P1-ST) [18]. The more evenly distributed temperature over the length of the tapered arm is evident. Note, the length of the arms in both actuators is 220 $\mu m,$ making the overall actuator length approximately 460 $\mu m.$	4-23
Figure 4-14.	(a) Illustration of a hot arm pair that shows the naming convention used to define the tapering geometry. (b) Simulated deflection curve as a function of the C/D ratio. Note: maximum deflection is produced by a C/D ratio of 1.32 [18]	4-24

Figure 4-15.	Illustration of actuator and cantilever beam arrangement for experimentally determining applied force. The length of the beam, $L$ , and the width of the beam, $w$ , are also shown.	4-25
Figure 4-16.	Schematic of an end-loaded cantilever beam arrangement used to determine the applied force from the bent-beam actuators [21]. The length of the beam, $L$ , the applied force, $F$ , and the deflected distance, $d$ , are shown	4-26
Figure 4-17.	Graphical representation of Equation (4.5), depicting the actuator force required to produce maximum deflection for a cantilever beam with three different lengths and the following common parameters: $E = 158$ GPa, $t = 3.2$ µm, and $w = 8$ µm.	4-29
Figure 4-18.	(a) Design layout of overlapping interrupter plates. (b) SEM image of fabricated overlapping interrupter plates. (c) SEM image of overlapping interrupter plates showing conformal topology	4-31
Figure 4-19.	SEM images showing (a) the connections between the latching mechanism and the actuator, and (b) the two components which make up the latching mechanism.	4-32
Figure 4-20.	Design layout of the "closed" interrupter, depicting the 4-μm² area where no coverage exists.	4-33
Figure 4-21.	Illustration of the change in aperture area as a result of actuator deflection. Notice the difference between the initial aperture area and the resulting aperture area.	4-34
Figure 4-22.	Graphical representation of the quadratic dependence of the actuator deflection on the aperture area in accordance with Equation (4.8). The red line indicates a realistic expectation for the aperture area based on the anticipated performance of the bent-beam actuators designed for the interrupter mechanism in this thesis.	4-35
Figure 4-23.	(a) One of the four actuator elements that make up the interrupter mechanism. The actuator is dimmed since it is not included in the free-body diagram. (b) Free-body diagram of the interrupter mechanism shown in (a). Only the (Poly1) plate, the linkage, and the latch component are considered in determining the required actuator force.	4-36

Figure 4-24.	Graphical representation of Equation (4.11) along with some comparisons between typical munition systems using the Mach numbers as provided by Table 2-1. Note: all aerodynamic heating temperature for these munition systems are below the melting point of polysilicon.  4-41
Figure 5-1.	SEM images of width test structures showing that a minimum beam width of 1 µm survived the fabrication process for both (a) the Poly1 beam, and (b) the Poly2 beam. However, the Poly2 beam does not look to have very much structural rigidity
Figure 5-2.	SEM images of the spacing test results for fabrication run #68: (a) Image of all three polysilicon layers with associated gap measurements, (b) Image of the Poly0 layer, (c) Image of the Poly1 layer, and (d) Image of the Poly2 layer. Note: the minimum spacing of 2 µm could clearly be fabricated in this process run5-4
Figure 5-3.	SEM image of the spacing test results for run #69 that includes the polysilicon layers – Poly0 (P0), Poly1 (P1), and Poly2 (P2). The numbers to the right represent the spacing between the two adjacent structures, in $\mu$ m. Again, the 2 $\mu$ m spacing is the minimum spacing gap that could be fabricated in this run. Clearly, the 1 $\mu$ m spacing could not be fabricated in this process
Figure 5-4.	Optical profiler measurement to determine the thickness of the deposited polysilicon layer (Poly0). Note: the value shown is for only one measurement, and the reported values in Table 5-1 shows the average thickness values based on multiple measurements
Figure 5-5.	20X magnification image of 400 $\mu$ m $\times$ 8 arm (straight and tapered) electrothermal actuators. Note: the tapered arms are visibly thicker in the center of the arms than the straight arms
Figure 5-6.	Measured resistance of the bent-beam electrothermal actuators.  The error bars indicate one standard deviation from the mean5-10
Figure 5-7.	(a) Bent-beam electrothermal actuator with N arms. (b) Equivalent circuit model of the N-arm actuator showing its reduction into a single resistive element with an equivalent resistance, $R_a$ , as described by Equation (5.2).

Figure 5-8.	Average deflection as a function of input power for nine 400 $\mu$ m $\times$ 8 tapered arm electrothermal actuators. The error bars indicate one standard deviation from the average deflection for each voltage step measured.	5-13
Figure 5-9.	Average deflection as a function of input power for all four different bent-beam electrothermal actuators. For a given input power, the 400 $\mu m \times 8$ straight arm actuator produced the largest deflection. Moreover, the actuators with 8 arms also produced a greater deflection for a given input power over those with 12 arms. Lastly, the tapered actuators produced less deflection than their straight armed counterparts.	5-14
Figure 5-10.	Performance-to-energy comparison between all four bent-beam electrothermal actuators. The deflection-to-power ratio at each voltage step is compared to show that the 400 $\mu$ m $\times$ 8 straight arm actuator does indeed have advantages, over the other actuators, if low power performance is desired.	5-14
Figure 5-11.	One set of bent-beam electrothermal actuators (400 $\mu$ m $\times$ 8 straight arms) designed adjacent to the force measuring cantilever beams of three different lengths: 100 $\mu$ m, 200 $\mu$ m, and 300 $\mu$ m.	5-15
Figure 5-12.	(a) Image of the 400 $\mu m \times 8$ tapered arm actuator at 0 V. (b) Image of the same actuator at 23 V and a maximum cantilever beam deflection of 11 $\mu m$ . Note: the dashed lines represent the initial beam location.	5-16
Figure 5-13.	SEM image of a 400 $\mu m \times 8$ straight arm actuator with a 100 $\mu m$ force measuring cantilever beam. The inset shows the 2.5 $\mu m$ gap that must be accounted for in determining the maximum deflection of the cantilever beam, along with the measured width of the beam	5-17
Figure 5-14.	Average output force for each type of bent-beam electrothermal actuator, along with one standard deviation from the calculated averages based on the two force data points (for the 100 $\mu$ m and 200 $\mu$ m cantilever beams) provided in Table 5-2.	5-20

Page

Figure 5-15.	(a) Equivalent circuit model for the interrupter mechanism, where $R_a$ is given by the actuators' resistance values shown in Figure 4-6. (b) Image of actual interrupter mechanism (just prior to activation) showing how the electrical circuit was connected. Note: this image is from Die #14, which uses four 400 $\mu$ m $\times$ 12 straight arm actuators.	5-23
Figure 5-16.	Measure resistance values for the complete interrupter mechanism, along with the standard deviation based on measurements of at least three separate devices.	5-24
Figure 5-17.	Input power as a function of the applied voltage for each interrupter mechanism. Consistent with the results seen in Section 5.2.1, the interrupter mechanism with the 400 $\mu$ m $\times$ 8 straight armed actuators has the lowest power requirements	5-25
Figure 5-18.	Operation of a MEMS interrupter mechanism at 50X magnification. This sequence of images shows Interrupter #3 at:  (a) 0 V, (b) 5 V, (c) 10 V, and (b) 15 V	-27
Figure 5-19.	Operation of Interrupter #1 at: (a) 0 V, and (b) 15 V. These images show center of interrupter mechanism at 20X magnification. Note: the expansion of the bent-beam actuator arms is visible in (b)	-27
Figure 5-20.	Operation of Interrupter #2 at: (a) 0 V, and (b) 15 V. These images show center of interrupter mechanism at 10X magnification. Again, note the expansion of the bent-beam actuator arms in (b)5	-28
Figure 5-21.	Maximum actuator deflection shown at 50X magnification. The inability of the actuator to move the fixed latching components limits the maximum deflection of each actuator to approximately 15 μm.	5-29
Figure 5-22.	Design layout of latching components for interrupter mechanism. The latching beams require a force of approximately 900 µN to produce the 5 µm deflection required for latching to occur. This force value is based on the length and width of the designed beam. Note: the latching beam thickness is a result of the stacked Poly1 + Poly design.	5-29

Figure	Page
C	<u> </u>

Figure 6-1.	Image of a 400 $\mu$ m $\times$ 8 tapered arm electrothermal actuator, fabricated in run #69, shown at 100X magnification. This figure shows that 2.5- $\mu$ m wide $\times$ 3.5- $\mu$ m thick arms could be fabricated in the PolyMUMPs process.	6-3
Figure 6-2.	SEM image showing interrupter mechanism. The fabricated spacing between the two structures of the same material layer was measured to 2.5 $\mu$ m (Designed spacing was 2 $\mu$ m.) This produced a "closed" aperture area of 6.25 $\mu$ m <sup>2</sup> (Designed to be 4 $\mu$ m <sup>2</sup> .) Note: the pseudo-guide rails that were formed on the Poly2 layer as a result of the spacing between the two Poly1 layers and the conformality of the fabrication process.	6-4
Figure 6-3.	(a) Alternative latching mechanism that was fabricated in PolyMUMPs run #68 using both Poly and Poly2. This latch was demonstrated by using a microprobe to push the structure until latching occurred. (b) Magnified view of (a) showing the two latching components are "latched" at only a 5 μm portion of the locking mechanism. However, the validity of the latching mechanism was clearly demonstrated, and better results could be obtained by optimizing this design.	6-8
Figure 6-4.	(a) SEM images showing fabricated features on the surface of the interrupter plates. All of the following features were designed to a diameter of 6 µm: dimples shown on both Poly1 and Poly2, Poly1 etch holes, Poly2 etch holes, and an inadvertent error – Poly1 etch hole under a Poly2 layer.	6-9
Figure A-1.	Carbon dioxide phase diagram showing the supercritical CO <sub>2</sub> drying cycle	A-3
Figure A-2.	Automatic supercritical CO <sub>2</sub> dryer used to prevent stiction in the MEMS dies used in this research effort.	A-4

# **List of Tables**

Table		Page
Table 2-1.	Typical Forces During Launch and Free Flight [1].	2-4
Table 4-1.	Summary of the bent-beam actuators tests described by Szabo [17]	. 4-21
Table 4-2.	Summary of the bent-beam actuator design parameters chosen for each of the interrupter mechanisms fabricated as part of this research effort.	. 4-25
Table 4-3.	Force required to move a single interrupter element consisting of the plate, linkage, and latch component	. 4-38
Table 5-1.	Comparison between the average thicknesses measured for several fabricated structures and the thickness data provided by MUMPs <sup>®</sup> for run #68 [3].	5-5
Table 5-2.	Summary of the data collected from the bent-beam actuator force measurement tests to include, the average maximum beam deflection (based on three actuators of each type), the standard deviation, and the calculated output force. Note: the calculated force for the 300 $\mu$ m beam is considered invalid because the required maximum beam deflection exceeds the maximum deflection capability of the actuator.	5-19
Table A-1.	Release procedures used for MEMS dies fabricated in this research effort	A-2
Table B-1.	PolyMUMPs Run #66 measured fabrication data [1]	B-1
Table B-2.	PolyMUMPs Run #67 measured fabrication data [1]	B-1
Table B-3.	PolyMUMPs Run #68 measured fabrication data [1]	B-2
Table B-4.	PolyMUMPs Run #69 measured fabrication data [1]	B-2

#### 1. Introduction

For the people that work around explosive weapons, safety is a vital concern that affects all facets of a weapon's life – from transportation, to storage, to maintenance, to buildup, to upload, to flight, and to release. The potential for a major mishap, to include both equipment and personnel, exists if a weapon is inadvertently armed during one of these operations. To ensure that the weapon is in an "armed" condition only when desired and in a "safe" condition at all other times is the function of the safe and arm device [1], which is an integral part of the weapon's fuze.

## 1.1 Safe and Arm Device Functional Description

The safe and arm (S&A) device is an element of the fuze, which is a critical component of all munition items. The fuze is responsible for initiating the sequence of steps that ultimately leads to weapon detonation. The method of initiation for a particular fuze depends on the intended launch environment, or the desired effect upon detonation. For example, fuzes can be designed to initiate the explosive train on impact, by sensing a relative proximity to a target, or by sensing depth of penetration through a target. This latter example applies to bunker busting-type weapons where it is desirable to penetrate through various levels of dirt and/or concrete barriers before detonation. A critical

requirement for fuzes is their high reliability standards that must be maintained throughout years of storage, maintenance, and use in a variety of surroundings. For instance, fuzes and their internal components need to endure extreme environmental conditions that range anywhere from large temperature fluctuations during many years of dormant storage to the high acceleration forces experienced both prior to and in the launch environment [2], [3]. Figure 1-1 shows several pictures of fuzes currently used for both air-to-air and air-to-ground munition systems. The S&A device is a component within each of these fuzes.

The S&A device has the essential function of preventing a premature detonation by eliminating the potential for energy to reach the main charge. This is accomplished by

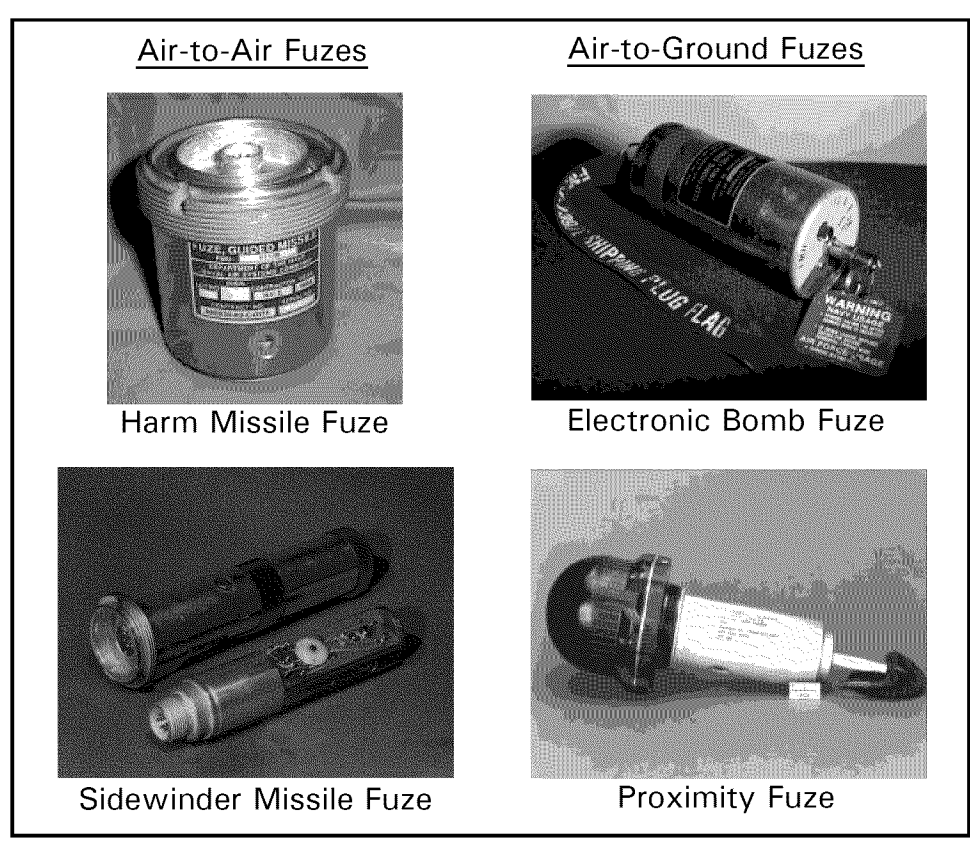


Figure 1-1. Fuzes currently being used in military weapons [4]. Safe and arm devices are a critical component within each of these fuzes.

eliminating a continuous path for the energy to propagate through the explosive train. Toward this objective, S&A devices often "interrupt" the explosive train by making use of in-line mechanisms as a way to prevent inadvertent arming. Figure 1-2 shows a schematic diagram of a generic explosive train that depicts the spatial relationship between explosive charges and the S&A device. Another function of the S&A device, equally important as preventing a continuous path, is allowing a continuous path. When a predetermined set of conditions are satisfied, the physical mechanisms (within the S&A device) that interrupt the explosive components are removed, thereby enabling the explosive energy to propagate toward the main charge, ultimately resulting in weapon detonation. In this case, an input energy source is detected by a detonator, which is a very sensitive explosive element designed to amplify a weak initial signal. The next explosive element is the lead charge, which represents the next stage of amplification. The booster charge depicts the final stage of amplification that provides the necessary explosive force to detonate the main charge [1]. To be effective, the device must remain

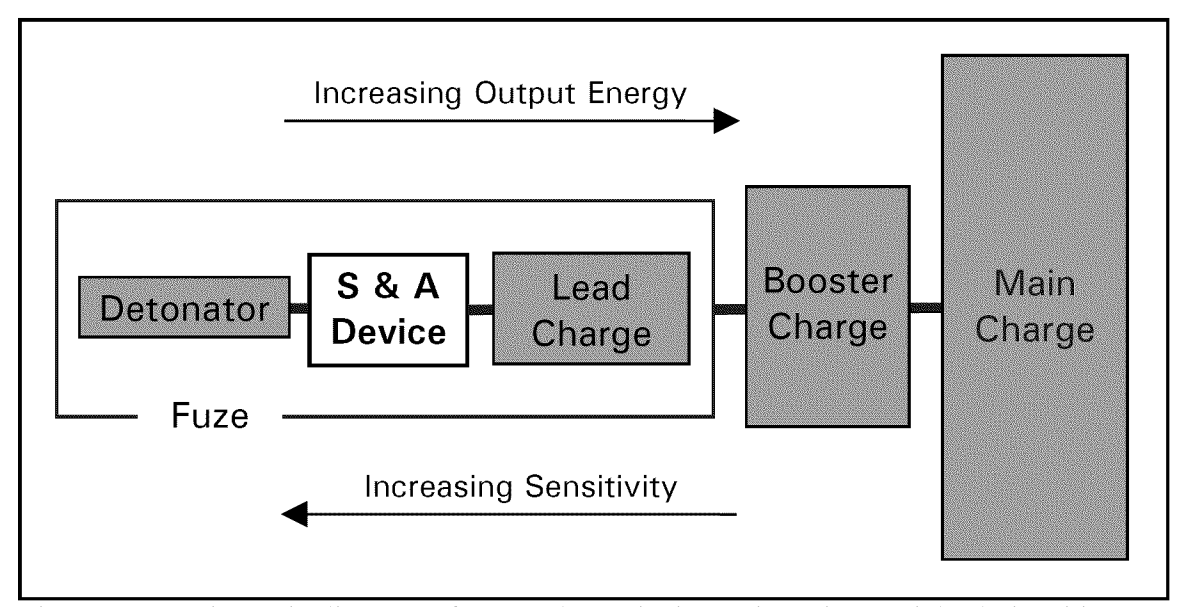


Figure 1-2. Schematic diagram of a generic explosive train. The spatial relationship between fuze, S&A device, and other charges is shown.

in a safe configuration during most of its lifetime, thus preventing an armed condition until the last possible instant. Additionally, the S&A device must be able to move very rapidly, and accurately, into the armed condition since most munitions travel at high velocities once launch has been initiated [5].

The "interruption" method used by manufacturers of S&A devices vary, but most call the mechanism that performs this function the interrupter. Interruption can be performed by misaligning the explosive components or by providing a physical barrier so that the explosive components cannot propagate through the explosive train in the case of an inadvertent initiation. Various levels of complexity can be designed into this interrupter mechanism to ensure it remains safe; however, device complexity usually has a direct impact on device reliability. More complex interrupter schemes have a greater potential to introduce single-point failure modes into the explosive train, which can result in a launched weapon that fails to detonate [6].

In order for the interrupter to move into the armed position, a specific sequence of events (for which the S&A device is designed) must be detected to ensure a valid launch command has occurred. This is typically achieved by ensuring at least two distinct environmental conditions are satisfied, which indicate an intentional detonation sequence has been initiated [7]. Care must be taken that the selected environmental stimuli will not be experienced in the munition lifecycle except when the munition is in the proper launch cycle. The launch cycle is defined as the period between when "the munition is irreversibly committed to launch" and some relatively short time after it leaves the weapon launch platform [7]. The launch platform could be an aircraft, ship, artillery tube, or rifle.

#### 1.2 Problem Statement

One of the issues facing the munitions community in recent years is the age of fuzes and their components in existing weapons systems. The reliability of these older fuzes tend to decrease over time, and existing systems will require components to be replenished in the coming years, either through product improvement or new development programs [8], [9]. In addition to finding replacement components for older weapons systems, new S&A devices need to be developed for munitions currently being acquired. Many designs that exist today use mechanisms that were designed over two decades ago and some designs are too complex and costly with respect to other improvements being made to modern weapon systems [10]. Modern munition items tend to be designed for more reliability and accuracy, and as such require a S&A device that achieves an equal, if not better, level of performance to ensure both infallible safety and lethal functionality.

Another problem, which compounds the issue of an aging stockpile, is that old S&A designs are difficult to reproduce since the industrial base that manufactures these devices is shrinking. From 1987 to 2001, the firms that produce electronic and electromechanical fuzes shrunk by over 80 percent (from 31 to 6) [2]. Additionally, the suppliers of Army fuzes have reduced in numbers from 20 to 5 since 1999 [11]. The military downsizing that occurred in the 1990's reduced the dollars available for munitions expenditures, and as a result many manufacturers stopped producing fuzes because it became less profitable [9], [11].

## 1.3 Proposed Solution

A common approach in designing modern weapon systems is to miniaturize munitions, which places a 'smaller is better' requirement on all components that make up a munition item, including the S&A device. Advances in solid-state fabrication techniques have made it possible to create micrometer-scale mechanical systems, which enable alternative design possibilities for fuze designers. Consequently, S&A devices designed using micro-electro-mechanical systems (MEMS) concepts become an obvious area to explore for potential exploitation. MEMS technology is based on the thoroughly refined fabrication methods used in the integrated circuit community. The processes used in fabricating integrated circuit devices using solid-state materials have been well proven over the last 50 years. Starting with the first transistor developed in 1947 by engineers at Bell Laboratories and the first integrated circuit demonstrated in 1958 by Texas Instruments [12], tremendous advances have been made in the material research and processing technologies that enable the complex electronic devices produced today.

The attractiveness of MEMS S&A devices for modern weapons systems is their inherent benefits over current macro-scale devices. One example is that their smaller feature size offers the advantage of decreased mass, which directly benefits enhanced range and maneuverability requirements. This can be shown by considering the scale factor, S, of an object. Mass is known to scale in relation to the volume of an object, therefore, the scale factor for mass is  $S^3$  [13]. For instance, consider a cube where the length of each edge is one meter. If each edge length is reduced to one micrometer ( $10^{-6}$  meter), the mass of the cube will decrease by  $1/10^{18}$  ( $S = 1/10^6$ ), or by a factor of  $10^{18}$ . On a more practical scale, consider the length of each edge scaling from one millimeter

 $(10^{-3} \text{ meter})$  to one micrometer  $(10^{-6} \text{ meter})$ . Applying the mass scale factor of  $S^3$  to this example, results in the mass decreasing by a factor of  $10^9$ .

Another example of the inherent benefits of MEMS devices is the higher fabrication volumes, which typically contributes to lower costs over time. The decrease in cost is a result of the capability to produce these devices in large volumes. This has been irrefutably witnessed in the processes used to fabricate integrated circuits, which are very similar to the processes used in MEMS fabrication. As a final example of inherent MEMS benefits, the lower part counts, that are generally characteristic of these devices, have a tendency to increase reliability over systems with a larger part count.

Clearly, if an S&A device, designed with components manufactured with MEMS techniques, could be successfully demonstrated, it would allow more design flexibility for the replenishment of fuze elements in current munitions, and enable additional approaches in the design of modern weapon systems. Additionally, MEMS-based S&A devices could be used for advanced munitions concepts, such as miniature weapons on unmanned aerial vehicles (UAV) and 'smart' bullets.

#### 1.4 Conclusion

This research effort will focus on an interrupter design concept created completely in a MEMS fabrication process. The Multi-User MEMS Processes (MUMPs®) fabrication process was used for all four design iterations submitted as part of this thesis. Each device uses polysilicon as the structural layers and hence the specific process provided by MUMPs® is called PolyMUMPs™. The PolyMUMPs process is a three-layer, general-purpose surface micromachining process that offers two releasable polysilicon layers and one metal layer [14].

Chapter 2 of this thesis will discuss some basic concepts that must be considered when designing a munition fuze, along with the forces typically encountered in military weapons. In addition, several micro-scale S&A devices currently being investigated will be presented. Chapter 3 will discuss some common devices used to initiate explosive trains, along with a look at a specific detonator device that has been fabricated using microelectronic fabrication techniques. Chapter 3 will conclude with some ideas on how to integrate the MEMS interrupter concept proposed in this research with a microdetonator device. Chapter 4 will discuss the theory involved in designing a MEMS interrupter mechanism, and the motivation for selecting the individual components that are incorporated into the final fabricated device. Chapter 5 will discuss the test results used to characterize the performance of the individual actuation mechanisms, along with the experimental results of the fabricated S&A interrupter device. Lastly, Chapter 6 will discuss the conclusions reached based on these experimental results and present some recommendations for future work in this area.